EAI Endorsed Transactions
on Energy Web

Research Article EAI.EU

# Multi-objective Optimization of Energy Storage Capacity for Wind-Solar Microgrids Based on Digital Twins and a TCN-SLSTM-MHA Hybrid Model

Tong Xia[1*], Jichao Ye[1], Yijia Lü[1], Xinwei Hu[1], Hui Huang[1], and Yonghai Xu[1]

[1]Lishui Power Supply Company, State Grid Zhejiang Electric Power Co., Ltd., Lishui, Zhejiang 323000, China

## Abstract

To address the challenges in wind-solar microgrids caused by the intermittency and volatility of renewable energy—such as power imbalance, unreasonable energy storage capacity configuration, and the difficulty in achieving coordinated optimization of economy, reliability, and environmental sustainability under limited capacity—a multi-objective energy storage capacity optimization method is proposed based on digital twin technology and a hybrid model combining Temporal Convolutional Network (TCN), Stacked Long Short-Term Memory Network (SLSTM), and Multi-Head Attention (MHA) mechanism (TCN-SLSTM-MHA). First, a digital twin model of the wind-solar microgrid is constructed to enable real-time mapping, monitoring, and simulation analysis between the physical system and its virtual counterpart, overcoming the limitations of traditional models in adapting to dynamic operational scenarios. Second, a TCN-SLSTM model is introduced, enhanced with the MHA mechanism to dynamically assign weights across time steps, thereby improving the accuracy of source (generation) and load forecasting. Finally, a multi-objective optimization function is established that simultaneously considers the minimization of Life Cycle Cost (LCC), maximization of Power Supply Reliability (PSR), and reduction of Carbon Emission Intensity (CEI), enabling the optimal determination of storage capacity. Experimental results demonstrate that, in terms of source-load forecasting, the proposed model improves prediction accuracy by 16.9% and 16.7%, respectively, compared to the conventional TCN-LSTM model. In energy storage capacity optimization, compared to the traditional weighted sum method, the proposed approach reduces LCC by 15.2%, increases PSR by 4.3%, and decreases CEI by 12.5%, validating the effectiveness and superiority of the proposed model.

**Keywords:** wind-solar microgrid; digital twin; TCN-SLSTM-MHA; energy storage capacity; multi-objective optimization

Received on 15 January 2026, accepted on 02 May 2026, published on 19 August 2026



doi: 10.4108/ew.14194

## 1. Introduction

As a distributed power generation system that efficiently utilizes renewable energy, wind-solar microgrids integrate renewable energy sources such as wind power and photovoltaic power. They can effectively reduce reliance on traditional fossil fuels and lower carbon emissions, garnering widespread attention and rapid development [1]. However, the intermittency, volatility, and uncertainty of wind and solar energy pose significant challenges to the stable operation of microgrids. These factors make it difficult to achieve precise matching between power generation and load demand, easily leading to power imbalance issues that affect system reliability and power quality [2]. Energy Storage Systems (ESS), as a key component of wind-solar microgrids, can store electrical energy during periods of surplus generation and release it during periods of insufficient supply, thereby performing

*Corresponding author. Email: xiatong84@sohu.com

peak shaving and valley filling functions. This effectively mitigates power fluctuations and enhances system stability and reliability. The rational allocation of energy storage capacity is crucial for the efficient operation of wind-solar microgrids [3]. Therefore, how to achieve the optimal allocation of energy storage capacity while accounting for the uncertainty of wind and solar power generation and load demand has become a research hotspot and a key issue in the field of wind-solar microgrids [4].

In response, numerous scholars both domestically and internationally have conducted research on the optimal allocation of energy storage capacity. The essence of optimizing energy storage capacity in wind-solar microgrids lies in achieving multi-objective trade-offs by optimizing the capacity, power allocation, and charge-discharge strategies of ESS while satisfying power balance constraints [5]. Existing studies are mostly based on deterministic power forecasting models, i.e., assuming that wind and solar output or load is known or expressed by physical formulas, and then employing various mathematical optimization methods to solve the problem. For example, Reference [6] proposes a power expression for wind power grid connection, constructs a capacity optimization model aimed at minimizing annual total cost, and solves it using an improved Archimedes optimization algorithm. Reference [7] utilizes mixed-integer linear programming for energy management in residential battery energy storage systems based on existing PV generation and load data. However, due to the stochastic nature of loads and renewable energy, as well as inevitable prediction errors, it may not be possible to accurately obtain renewable energy generation output or load power [8]. Furthermore, the use of physical formulae often fails to accurately reflect the system's actual operating conditions in practical applications, leading to biased optimization results that struggle to meet the requirements for reliable and economical operation of microgrids [9]. Therefore, it is necessary to conduct research on energy storage capacity optimization for wind-solar microgrids by integrating wind and solar power and load forecasting methods.

Wind, solar power, and load forecasting serve as critical inputs for energy storage capacity optimization. Forecasting methods can be categorized into physics-model-driven [10–12] and data-driven [13–15] approaches. With the rapid advancement of artificial intelligence technology, data-driven forecasting methods have demonstrated significant advantages in addressing uncertainty issues [16]. Temporal Convolutional Networks (TCN) [17] and Long Short-Term Memory Networks (LSTM) [18], as two important deep learning models, have been widely applied in the field of time series forecasting. To fully leverage the strengths of both, the TCN-LSTM model—a combination of TCN and LSTM—has emerged, capable of effectively enhancing the forecasting capability for complex time series data [19–20]. However, the fixed kernel size of TCN limits the extraction of multi-scale features, while the unidirectional recurrent units and gating mechanisms of LSTM do not sufficiently capture local critical information; thus, the combined TCN-LSTM model still requires further optimization.

Digital Twin (DT) technology, as an emerging cutting-edge technology, enables real-time mapping, monitoring, analysis, and optimization of physical entities by constructing virtual models that closely resemble them [21–22]. Introducing Digital Twin technology into the field of wind-solar microgrids can provide new insights and methods for optimizing energy storage capacity [23]. Specifically, by constructing high-fidelity virtual representations of physical entities, digital twin technology provides a platform for dynamic evolution and real-time decision-making support for microgrids, thereby enhancing system operational efficiency and reliability. Relevant studies have preliminarily validated the application potential of digital twins in microgrids. For example, Reference [24] uses digital twin technology to diagnose faults in microgrid clusters; Reference [25] combines digital twins with reinforcement learning to optimize energy management strategies for microgrids; and Reference [26] constructs a digital twin model of an Integrated Energy System (IES) and employs machine learning to achieve day-ahead scheduling optimization. In wind-solar microgrids, digital twin technology enables precise modeling of key components such as wind turbines, photovoltaic cells, energy storage systems, and loads. By collecting real-time system operation data via IoT technology, it facilitates synchronized updates and interaction between the virtual model and the physical system [27]. Based on this, the digital twin model enables simulation and modeling of different energy storage capacity configurations to comprehensively evaluate the system's operational performance under various operating conditions, thereby providing a more accurate and reliable basis for decision-making regarding energy storage capacity optimization.

Based on existing research, this paper proposes a multi-objective optimization method for energy storage capacity in wind-solar microgrids based on digital twins and a TCN-SLSTM-MHA hybrid model. First, a digital twin model of the microgrid is constructed using digital twin technology to enable real-time monitoring and simulation analysis of the system's operational status; then, a TCN-SLSTM-MHA hybrid model is developed to achieve high-precision forecasting of wind and solar power generation and load demand, providing accurate data support for energy storage capacity optimization; Finally, an optimization function is established that comprehensively considers multiple objectives, including Life Cycle Cost (LCC), Power Supply Reliability (PSR), and Carbon Emission Intensity (CEI), to optimize the energy storage capacity and achieve a good balance between reliability and economic efficiency in the wind-solar microgrid. Through analysis of practical case studies, the effectiveness and superiority of the proposed model and methods are verified, providing a scientific basis and technical support for the rational configuration of energy storage capacity in wind-solar microgrids.

## 2. Overall Framework of the Optimization Method

The overall framework of the multi-objective optimization method for energy storage capacity in wind-solar microgrids based on digital twins and the TCN-SLSTM-MHA hybrid model is shown in Figure 1.

The overall framework of the optimization method can be divided into the digital twin layer, the prediction layer, and the multi-objective optimization layer, with the three layers achieving synergy through a closed-loop process of data, prediction, optimization, and verification. The digital twin layer perceives physical data in real time, constructs a high-fidelity virtual model after preprocessing, and generates dynamic scenarios incorporating wind and solar fluctuations. This addresses the issue of traditional models' insufficient adaptability to actual operating scenarios and provides reliable input for the prediction layer. The prediction layer utilizes the high-quality data output by the digital twin. It extracts multi-timescale features via a multi-scale TCN, optimizes long-term dependency modeling using an SLSTM, and then fuses features through an MHA to achieve high-precision forecasts of wind and solar power and load, thereby providing critical data support for the optimization layer. The multi-objective optimization layer sets Life Cycle Cost (LCC), Power Supply Reliability (PSR), and Carbon Emission Intensity (CEI) as objectives. Under constraints such as power balance, it uses the Improved Non-dominated Sorting Genetic Algorithm II (NSGA-II) to determine the optimal energy storage capacity, which is then fed back to the digital twin layer to verify the feasibility of the solution, ultimately achieving a balance between economic efficiency and reliability in the energy storage configuration of the wind-solar microgrid.

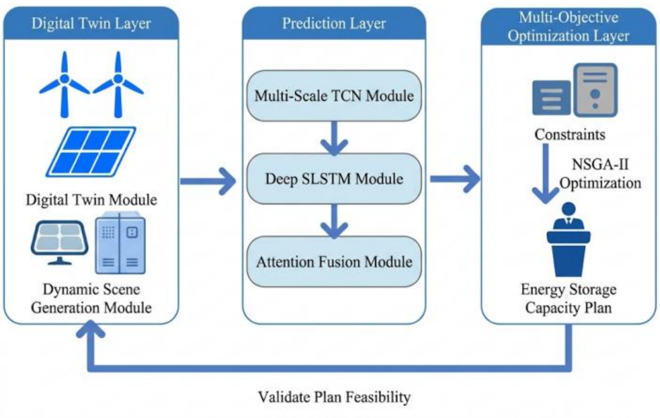


**Figure 1.** Overall framework of optimization methods

## 3. Wind-Solar Microgrid Modeling Incorporating Digital Twins

### 3.1. Digital Twin System Architecture Design

The Digital Twin of Wind-Solar Micro Grid (DT-WSMG) adopts a four-layer architecture comprising physical, virtual, data, and service layers, as shown in Figure 2. Its core functions include real-time sensing, high-fidelity modeling, dynamic mapping, and intelligent decision-making.

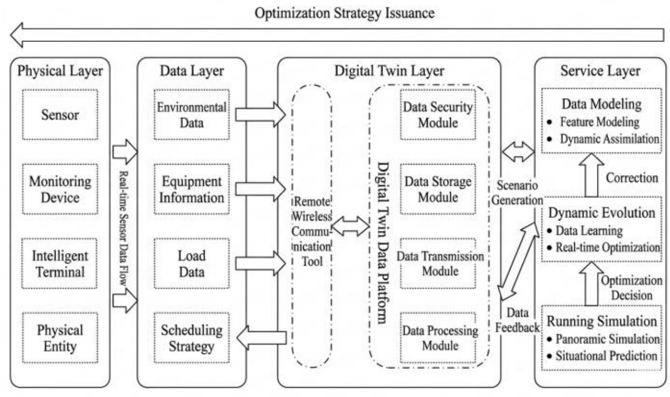


**Figure 2.** DT-WSMG architecture

The layers are as follows:

Physical Layer: Includes photovoltaic arrays, wind turbines, energy storage devices, loads, and energy conversion equipment. The mathematical model parameters for core components such as photovoltaic arrays and wind turbines (e.g., I-V characteristic curves for solar panels and power curves for wind turbines) are derived from measured data manuals provided by equipment manufacturers. These models are calibrated under offline operating conditions prior to deployment to ensure the validity of the underlying physical models.

Data Layer: Data such as solar and wind power output, energy storage State of Charge (SOC), and load power are collected in real time via a sensor network. After noise reduction and normalization through edge computing, the data is stored in a database.

Twin Layer: A microgrid physical model is built using Simulink, with parameters corresponding one-to-one with the devices in the physical layer.

Service Layer: Integrates prediction models, optimization algorithms, and visualization modules. Through the digital twin engine, it enables bidirectional interaction between physical and virtual data, supporting a closed-loop decision-making process of prediction-optimization-verification.

Physical Quantities → Virtual Model (Data-Driven): Real-time mapping of wind speed, solar irradiance, temperature, PV array output ($P_{pv}$), wind turbine output ($P_{wt}$), energy storage system State of Charge (SOC), and load power ($P_{load}$), etc.

Virtual Model → Physical System (Decision Feedback): Maps the optimal energy storage capacity configuration ($E_{bat}$, $P_{pcs}$) and corresponding charge/discharge strategies calculated by the optimization layer back to the physical system for simulation verification.

## 3.2. Dynamic Scenario Generation and Mapping Mechanism

To simulate the uncertainties in the actual operation of a microgrid, the digital twin system generates dynamic scenarios across multiple time scales. This paper employs correlation modeling based on Copula functions and Monte Carlo sampling to generate dynamic scenarios, thereby reducing uncertainties caused by inaccurate estimates of the correlation between wind and solar power outputs. The specific steps are as follows:

(1) Use historical data to fit the probability distributions of wind and solar power output, where photovoltaic output $P_{wt}$ follows a Beta distribution and wind power output $P_{wt}$ follows a Weibull distribution:

$$P_{\mathrm{PV}} \sim BETA(A_{\mathrm{PV}}, B_{\mathrm{PV}}) \quad (1)$$

$$P_{\mathrm{wt}} \sim \mathrm{Weibull}(k,c) \quad (2)$$

where: $\alpha_{pv}$ and $\beta_{pv}$ are the shape parameters of the Beta distribution; $k$ is the shape parameter of the Weibull distribution; and $c$ is the scale parameter.

(2) Describe the joint distribution of Ppvand Pwtusing a copula function; the Gumbel copula is selected to capture the non-negative correlation:

$$C(u,v;\theta)=exp[-((-lnu)^{\theta}+-lnv)^{\theta})^{1/\theta}] \quad (3)$$

Where: $\theta \geq 1$ is the correlation coefficient; $\theta = 1$ indicates independence, and $\theta \to \infty$ indicates perfect correlation.

(3) Generate N sets of wind and solar power output scenarios via Monte Carlo sampling. Combining these with the load forecast curve $P_{(load,i)t}$, we obtain a set of dynamic operation scenarios for the microgrid and the expression for each scenario:

$$\Omega=\{\Omega_1, \Omega_2, ..., \Omega_N\} \quad (4)$$

$$\Omega_I = \{P_{\mathrm{PV},I}(T), P_{\mathrm{WT},I}(T), P_{\mathrm{LOAD},I}(T)\}_{T=1}^{T} \quad (5)$$

The generated set of dynamic scenarios $\Omega$ is standardized and transmitted via a JSON-formatted API to the TCN-SLSTM-MHA prediction layer, with an input dimension of [N, T, 3].

# 4. TCN-SLSTM-MHA Hybrid Source-Load Forecasting Model

As shown in Figure 3, the TCN-SLSTM-MHA hybrid model consists of an input layer, a TCN layer, an SLSTM layer, an attention fusion layer, and an output layer. It enhances the accuracy of generation and load forecasting through multi-scale feature extraction and long-term dependency modeling.

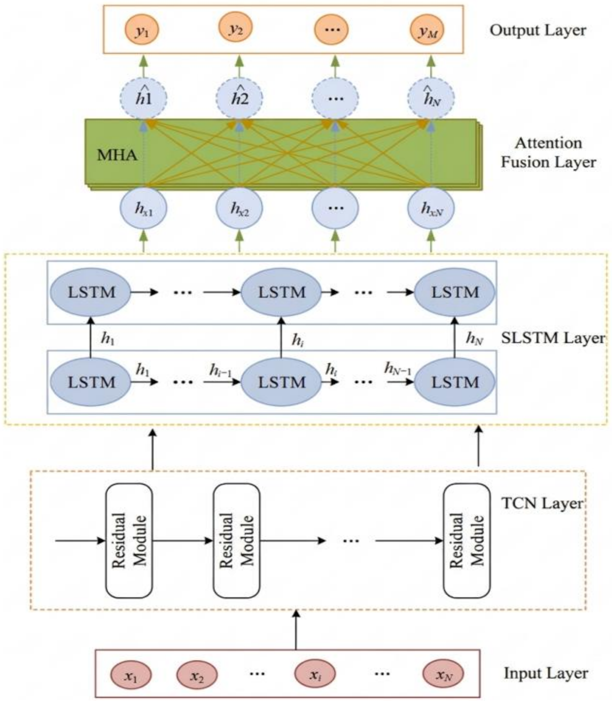


**Figure 3.** TCN-SLSTM-MHA hybrid model

## 4.1. TCN Layer

The core technology of TCN lies in the use of Dilated Causal Convolution (DCC) as the temporal convolution layer to extract temporal features from time series. In causal convolution, all data in the temporal dimension follow strict causal relationships, ensuring the sequential nature of time series information. To enhance the model's memory capacity for time series data, it is necessary to increase the depth of the convolutional layers or expand the size of the convolutional kernels. However, this leads to an increase in the number of model parameters, making training more challenging. Dilated convolution effectively addresses the limitations of causal convolution. By introducing a dilation factor, it enables non-contiguous convolution operations across longer time windows, allowing the convolution kernel to cover a time span wider than its own length. This enables the extraction of temporal features over a longer time span while maintaining a smaller number of convolution layers. The principle of DCC can be expressed as:

$$G(t)=\sum_{r=0}^{s-1} F_n(r)X_{t-dr} \quad (6)$$

Where: $G(t)$ denotes the output of the convolutional layer at time $t$; $F_n(r)$ denotes the weight parameters of the nth convolutional kernel at position $r$; $X_{t-dr}$ denotes the value of the input sequence at position $t-dr$; $d$ denotes the dilation factor; $s$ denotes the size of the convolutional kernel.

The TCN is composed of stacked residual blocks, each of which consists of two identical convolutional units. Each convolutional unit comprises a DCC unit, a weight normalization unit, an ReLU unit, and a dropout unit, as shown in Figure 4. To address the vanishing gradient problem in deep neural networks, residual connections are introduced into the residual blocks. These connections sum the input data with the output of the deep neural network to serve as the input for the next stage.

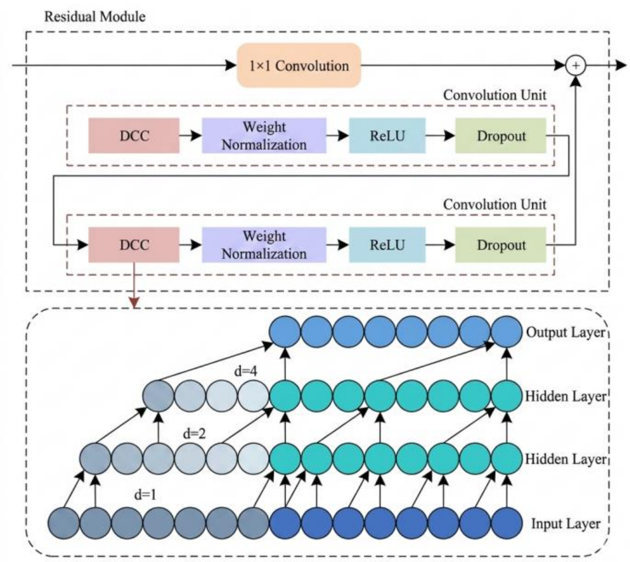


**Figure 4.** Structure of the residual block

## 4.2. SLSTM Layer

SLSTM constructs a deep recurrent neural network (RNN) structure by stacking and connecting multiple LSTM layers. Its core idea is to increase the depth of the LSTM network, enabling the model to extract features from low-level to high-level in sequence data layer by layer, thereby more efficiently capturing long-range dependencies and complex patterns. The structure is shown in Figure 5.

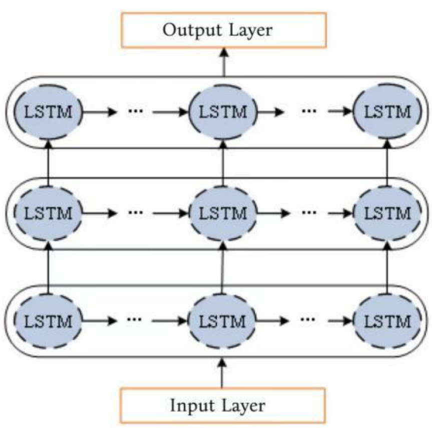


**Figure 5.** Structure of SLSTM

The internal computations within each LSTM layer are consistent with those of a traditional LSTM, dynamically regulating the retention and propagation of information through the gating mechanisms of the input gate, forget gate, and output gate. Taking the kth layer as an example, its computation at time step t includes:

Forget gate:

$$F_{K,T} = \Sigma(W_F^{(K)}[H_{K,T\text{-}1}, X_T]+B_F^{(K)}) \tag{7}$$

where: $W_f$ is the weight matrix, $b_f$ is the bias term, $h_t$ is the hidden state at the previous time step, $x_t$ is the current input, and $\sigma$ is the sigmoid function.

Input Gate:

$$i_{k,t} = \sigma(W_i^{(k)}[h_{k,t\text{-}1}, x_t]+b_i^{(k)}) \tag{8}$$

Where: $W_i$ is the weight matrix, and bi is the bias term.

Candidate cell state:

$$\hat{c}_{k,t} = tanh(W_c^{(k)}[h_{k,t\text{-}1}, x_t]+b_c^{(k)}) \tag{9}$$

Where: $W_c$ is the weight matrix, and $b_c$ is the bias term.

Cell state update:

$$c_{k,t} = f_{k,t} \bullet c_{k,t\text{-}1} + i_{k,t} \bullet \hat{c}_{k,t} \tag{10}$$

Where: $c_{t\text{-}1}$ is the cell state at the previous time step.

Output gate:

$$o_{k,t}=\sigma(W_o^{(k)}[h_{k,t\text{-}1},x_t]+b_o^{(k)}) \tag{11}$$

Where: $W_o$ is the weight matrix, and $b_o$ is the bias term.

Hidden state:

$$h_{k,t} = o_{k,t} \bullet tanh(c_{k,t}) \tag{12}$$

Where: $tanh$ denotes the hyperbolic tangent function.

## 4.3. Attention Fusion Layer

To further optimize the fusion of multi-scale features and time-dependent features, the MHA is designed to dynamically assign importance weights to each time step, which are ultimately integrated into a comprehensive representation through a concatenation operation, as shown in Figure 6.

The formulas for the query, key, and value vectors are as follows:

$$Q = X_{tcn} + b_q \tag{13}$$

$$K = W_k X_{tcn} + b_k \tag{14}$$

$$V = W_v X_{tcn} + b_v \tag{15}$$

Where: $X_{tcn}$ is the output matrix of the TCN layer; $W_q$, $W_k$, and $W_v$ are the weight matrices for $Q$, $K$, and $V$, respectively; and $b_q$, $b_k$, and $b_v$ are the corresponding bias terms.

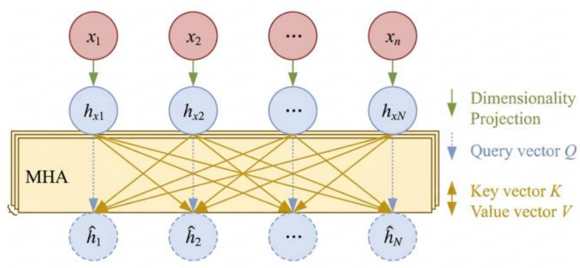


**Figure 6.** Structure of MHA

The attention formula is shown below:

$$head_i = Attention(Q_i, K_i, V_i) = softmax(\frac{Q_i K_i^T}{\sqrt{d_k}})V_i \quad (16)$$

$$MultiHead(Q,K,V)=Concat(head_1, ..., head_h)W^O \quad (17)$$

Where: $d_k$ is the dimension of each head, $d_k = \frac{d_{model}}{h}$, $d_k$ is the dimension of the hidden layer, $h$ is the number of attention heads, and $W^O$ is the linear transformation matrix.

## 4.4. Model Training Settings.

The model uses Mean Squared Error (MSE) as the loss function and is trained using the Adam optimizer, as shown in the following formula:

$$L=\frac{1}{N}\sum_{i=1}^{N}(P_{\mathrm{pred},i} - P_{\mathrm{true},i})^2 \quad (18)$$

Where: N is the number of training samples; $P_{pred,i}$ and $P_{true,i}$ represent the predicted and true values, respectively.

To prevent overfitting, an $L2$ regularization term $\lambda\|\theta\|_2^2$ ($\lambda$=0.01) and an early stopping mechanism (training stops if the validation set loss does not decrease for 5 consecutive epochs) are introduced.

# 5. Multi-objective Optimization Model for Energy Storage Capacity

## 5.1. Objective Function

This paper sets the *LCC*, *PSR*, and *CEI* of the energy storage system as optimization objectives.

*LCC* includes initial investment cost $C_{inv}$, operation and maintenance cost $C_{OM}$, and decommissioning and recycling cost $C_{rec}$, calculated as follows:

$$LCC = C_{\mathrm{inv}} + C_{\mathrm{OM}} + C_{\mathrm{rec}} \quad (19)$$

$$C_{\mathrm{inv}} = c_{\mathrm{bat}} \cdot E_{\mathrm{bat}} + c_{\mathrm{pcs}} \cdot P_{\mathrm{pcs}} \quad (20)$$

$$C_{\mathrm{OM}} = (c_{\mathrm{bat}} \cdot E_{\mathrm{bat}} + c_{\mathrm{pcs}} \cdot P_{\mathrm{pcs}}) \cdot \gamma \cdot T_{\mathrm{life}} \quad (21)$$

$$C_{\mathrm{rec}} = \delta \cdot (c_{\mathrm{bat}} \cdot E_{\mathrm{bat}} + c_{\mathrm{pcs}} \cdot P_{\mathrm{pcs}}) \quad (22)$$

In the formula: $c_{\mathrm{bat}}$ is the unit capacity cost of the battery, $E_{bat}$ is the battery capacity, $c_{pcs}$ is the unit power cost of the power converter, $P_{pcs}$ is the power of the power converter, $\gamma$ is the annual O&M rate, $T_{life}$ is the system lifespan (assumed to be 10 years), and $\sigma$ is the decommissioning and recycling coefficient.

The PSR uses the Loss of Power Probability (LOPP) and Loss of Energy Expectation (LOEE) to comprehensively characterize the system, as shown in the following formula:

$$PSR=1-(\alpha \cdot LOPP+(1-\alpha) \cdot LOEE) \quad (23)$$

where: $\alpha$ is the weighting coefficient.

The CEI considers the carbon footprint of grid-purchased electricity and the full life-cycle carbon footprint of the energy storage system. The calculation formula is as follows:

$$CEI=\frac{(\lambda_{\mathrm{grid}} \cdot E_{\mathrm{grid}} + \lambda_{\mathrm{bat}} \cdot E_{\mathrm{bat}})}{E_{\mathrm{load}}} \quad (24)$$

Where: $\lambda_{grid}$ is the carbon emission factor per unit of grid-purchased energy, $\lambda_{bat}$ is the carbon emission factor per unit of battery capacity, and $E_{load}$ is the total load energy.

## 5.2. Constraints

The power balance constraint is given by the following formula:

$$P_{\mathrm{pv}}(t)+P_{\mathrm{wt}}(t)+P_{\mathrm{ess}}^{\mathrm{dis}}(t)=P_{\mathrm{load}}(t)+P_{\mathrm{ess}}^{\mathrm{ch}}(t)+P_{\mathrm{grid}}(t) \quad (25)$$

Where: $P_{\mathrm{ess}}^{\mathrm{ch}}(t)$ and $P_{\mathrm{ess}}^{\mathrm{dis}}(t)$ represent the charging/discharging power of the energy storage system at time t, respectively; $P_{\mathrm{pv}}(t)$ and $P_{\mathrm{wt}}(t)$ represent the power generated by photovoltaic and wind power, respectively; $P_{\mathrm{load}}(t)$ represents the load; and $P_{\mathrm{grid}}(t)$ represents the power exchanged with the grid.

The energy storage *SOC* constraint is given by the following equation:

$$SOC_{\mathrm{min}} \leq SOC(t)=SOC(t-1)+\eta_{\mathrm{ch}} \cdot \frac{P_{\mathrm{ess}}^{\mathrm{ch}}(t)}{E_{\mathrm{bat}}} \cdot \Delta t-\frac{P_{\mathrm{ess}}^{\mathrm{dis}}(t)}{\eta_{\mathrm{dis}} \cdot E_{\mathrm{bat}}} \cdot \Delta t \leq SOC_{\mathrm{max}} \quad (26)$$

Where: $\eta_{\mathrm{ch}}$ = 0.95 (charging efficiency), $\eta_{\mathrm{dis}}$ = 0.9 (discharging efficiency),$\Delta t$ = 1 hour,$SOC_{\mathrm{min}}$ = 0.1, $SOC_{\mathrm{max}}$ = 0.9.

The equipment capacity constraint formula is shown below:

$$0 \leq P_{\mathrm{ess}}^{\mathrm{ch}}(t) \leq P_{\mathrm{pcs}} \quad (27)$$

$$0 \leq P_{\mathrm{ess}}^{\mathrm{dis}}(t) \leq P_{\mathrm{pcs}} \quad (28)$$

## 5.3. Multi-objective Optimization Solution

The improved NSGA-II algorithm is used to solve the multi-objective optimization problem. *The crossover probability* $P_c$ and *mutation probability* $P_m$ are dynamically adjusted based on population diversity to avoid premature convergence. The formulas for the dynamic adjustment strategy of *the crossover probability* $P_c$ and *mutation probability* $P_m$ are shown below:

$$P_c = 0.9\times(1 - \text{number of iterations / total number of iterations}) \quad (29)$$

$$P_m = 0.1\times\text{number of iterations / total number of iterations)} \quad (30)$$

Additionally, an external archive is introduced to store non-dominated solutions, and a reference point selection mechanism is employed to guide the population toward the Pareto front. The penalty function method is adopted to transform the constraints into penalty terms in the objective function, as shown in the following formula:

$$F = L + \rho \cdot \sum_{j=1}^{M} \max(0, g_j(x))^2 \quad (31)$$

where: $L$ is the original objective function, $\rho$ is the penalty coefficient (set to 1000), and $g_j(x)$ is the jth inequality constraint.

The optimized energy storage capacity scheme is fed back to the digital twin layer, where it is simulated for a full year of operation in the virtual model to verify the scheme's reliability under extreme wind and solar fluctuation scenarios. If verification fails (e.g., curtailment rate > 5%), a new dynamic scenario is generated for iterative optimization.

The improved NSGA-II algorithm does not require manually setting fixed weights; instead, it directly searches for a set of Pareto-optimal solutions. When making decisions in specific scenarios, the entropy weighting method is used to objectively calculate weights, as shown in the following formula:

$$w_j=\frac{1-e_j}{\sum_{k=1}^{m}(1-e_k)} \tag{32}$$

$$e_j=-\frac{1}{\ln n}\sum_{i=1}^{n}p_{ij}\ln p_{ij} \tag{33}$$

$$p_{ij}=\frac{x_{ij}}{\sum_{i=1}^{n}x_{ij}} \tag{34}$$

Where: $w_j$ is the weight of the jth objective (e.g., LCC, PSR, CEI); $e_j$ is the information entropy; $x_{ij}$ is the value of the jth objective function for the ith solution.

## 6. Experimental Analysis

A wind-solar microgrid in a certain region was selected as the experimental subject. This microgrid comprises 10 1.5 MW wind turbines, a 500 kW photovoltaic array, an energy storage system, and various user loads. The experimental dataset is derived from the microgrid's historical operational data from January 1, 2020, to December 31, 2022, with a sampling interval of 1 hour. It comprises a total of 26,280 data records, covering parameters such as wind speed, irradiance, temperature, wind and solar power output, load power, and energy storage SOC. The capacity planning problem for the energy storage system addressed in this paper is a medium- to long-term optimization problem, with decision-making primarily based on daily or hourly energy balance. Therefore, historical operational data with a 1-hour sampling interval was used, and through the construction of sliding window samples and data preprocessing, the temporal characteristics of the time series were effectively extracted. The dataset was divided into training, validation, and test sets in a 7:2:1 ratio to ensure uniform distribution of data across all seasons. The experimental environment used in this study is shown in Table 1.

Table 1. Experimental Environment

| Name | Parameter |
|---|---|
| Processor | Intel Xeon Platinum 8592+ |
| Memory | 256GB |
| Graphics Card | RTX 5090 |
| Operating System | Windows 10 |
| Programming Language | Python 3.8 |
| Learning Framework | TensorFlow 2.6 |
| Data Analysis Tools | NumPy |
| Visualization Tools | Matplotlib |

The digital twin model collects data in real time via 32 sensors deployed in the microgrid. The sampling frequency matches that of the historical data, ensuring synchronization between the virtual model and the physical system. During the data preprocessing stage, median filtering is used to remove noise, and cubic spline interpolation is applied to fill in missing values, ultimately forming a continuous and complete time-series dataset.

### 6.1. Wind and Solar Power and Load Forecasting Experiment

#### 6.1.1. Experimental Setup and Preprocessing

To validate the predictive performance of the TCN-SLSTM-MHA hybrid model, the following comparison models were selected:

(1) TCN Model: Single layer, convolution kernel size 3, stranding rate [1,2,4], 64 hidden units;

(2) LSTM Model: Single layer, 64 hidden units, dropout rate 0.2;

(3) SLSTM Model: 3 stacked layers, 64 hidden units per layer, dropout rate 0.2;

(4) TCN-LSTM hybrid model: TCN (parameters as above) connected in series with LSTM (parameters as above);

(5) ARIMA model: $p$=3, $d$=1, $q$=2 (determined using the AIC criterion).

The raw data contains three types of noise interference: (1) impulsive outliers caused by sensor failures, accounting for 1.2%; (2) temporal misalignments caused by communication delays, accounting for 0.8%; (3) random fluctuations caused by environmental electromagnetic interference, accounting for 3.5%.

To address these issues, the following preprocessing workflow is adopted:

Step 1: Outlier Detection and Correction: Identify impulse-type outliers based on the 3σ criterion. For samples falling outside the range of ±3 standard deviations from the mean, correct them using the weighted average of the four adjacent time points, with weights following a Gaussian distribution based on temporal distance;

Step 2: Temporal Alignment: Misaligned data is corrected using a timestamp matching algorithm, and missing timestamps are supplemented via linear interpolation;

Step 3: Noise Reduction: A combination of wavelet denoising and Kalman filtering effectively removes random noise, improving the signal-to-noise ratio by 28.6%. The db4 wavelet possesses good regularity and compact support properties, enabling it to effectively match the non-stationary characteristics of wind and solar load signals, making it a common choice for power signal denoising. Based on the sampling frequency and the signal's primary frequency components, five decomposition levels were selected to effectively remove noise while preserving the trend. The first-order linear model formula for Kalman filtering is shown in Equation (35):

$$x_k = Ax_{k-1} + w_k \tag{35}$$

Where: the state variable $x_k$ is the signal value to be denoised, $A = 1$, and $w_k$ is the process noise.
The preprocessed data is normalized to the range [0,1] using the following formula:

$$x_{\text{norm}} = \frac{(x - x_{\min})}{(x_{\max} - x_{\min})} \tag{36}$$

where: $x_{\min}$ and $x_{\max}$ are the minimum and maximum values of the sample data, respectively.

Root Mean Squared Error (RMSE), Mean Absolute Error (MAE), and Coefficient of Determination ($R^2$) are used as evaluation metrics, with the formulas shown below:

$$RMSE(P_{\text{true}}, P_{\text{pred}}) = \sqrt{\frac{1}{n}\sum_{i=1}^{n}(P_{\text{true},i} - P_{\text{pred},i})^2} \tag{37}$$

$$MAE(P_{\text{true}}, P_{\text{pred}}) = \frac{1}{n}\sum_{i=1}^{n}|P_{\text{true},i} - P_{\text{pred},i}| \tag{38}$$

$$R^2(P_{\text{true}}, P_{\text{pred}}) = 1 - \frac{\sum_{i=1}^{n}(P_{\text{true},i} - P_{\text{pred},i})^2}{\sum^{n}(P_{\text{true},i} - \bar{P})^2} \tag{39}$$

Where: $n$ is the number of samples; $P_{pred}$ and $P_{true}$ are the predicted and true values, respectively; and $\bar{P}$ is the sample mean.

### 6.1.2. Experimental Setup and Preprocessing

1) Wind and Solar Power Forecasting

Table 2 shows the comparison of wind and solar power output prediction performance across different models. The RMSE for wind power prediction using TCN-SLSTM-MHA is 23.6 kW, which is 18.3% lower than that of TCN-LSTM and 32.4% lower than that of LSTM; the RMSE for solar power prediction is 15.8 kW, which is 15.5% lower than that of TCN-LSTM and 58.3% lower than that of ARIMA. The $R^2$ values all exceed 0.92, indicating that the model has a stronger explanatory power for wind and solar power output.

Table 2. Comparison of performance indicators for wind and solar power output prediction

| Model | Wind Power | | | Solar | | |
|---|---|---|---|---|---|---|
| | RMSE | MAE | $R^2$ | RMSE | MAE | $R^2$ |
| ARIMA | 68.5 | 52.3 | 0.61 | 37.9 | 29.4 | 0.65 |
| TCN | 35.2 | 27.8 | 0.83 | 22.4 | 17.6 | 0.86 |
| LSTM | 34.9 | 26.5 | 0.84 | 21.7 | 16.0 | 0.87 |
| SLSTM | 30.2 | 23.1 | 0.88 | 19.3 | 14.8 | 0.89 |
| TCN-LSTM | 28.9 | 21.5 | 0.89 | 18.7 | 14.2 | 0.90 |
| TCN-SLSTM-MHA | 23.6 | 18.2 | 0.93 | 15.8 | 11.9 | 0.92 |

Note: The units for RMSE and MAE are both kW; the same applies below.

Figure 7 shows the predicted output of wind and solar power from different models (using data from a typical day). The TCN-SLSTM-MHA hybrid model exhibits the best fit with the actual output curve; particularly during periods of high output volatility, its tracking performance is significantly superior to that of other models.

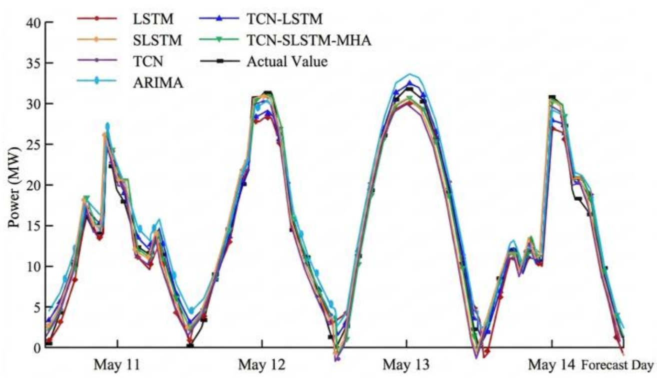


**Figure 7.** Prediction results of wind and solar power output by different models

2) Load Forecasting

The comparison of load forecasting performance metrics is shown in Table 3. The TCN-SLSTM-MHA hybrid model achieved an RMSE of 12.5 kW for load forecasting, a 16.7% reduction compared to the TCN-LSTM model, with an $R^2$ of 0.94, indicating that the model effectively captures the periodic and stochastic characteristics of the load.

Table 3. Comparison of load forecasting performance indicators

| Model | RMSE | MAE | $R^2$ |
|---|---|---|---|
| ARIMA | 38.2 | 29.7 | 0.72 |
| TCN | 18.6 | 14.3 | 0.88 |
| LSTM | 17.9 | 13.8 | 0.89 |
| SLSTM | 15.7 | 12.1 | 0.91 |
| TCN-LSTM | 15.0 | 11.5 | 0.92 |
| TCN-SLSTM-MHA | 12.5 | 9.8 | 0.94 |

Figure 8 compares the load forecast curves for typical days across different seasons. The TCN-SLSTM-MHA hybrid model exhibits the smallest prediction errors for both peak and off-peak loads.

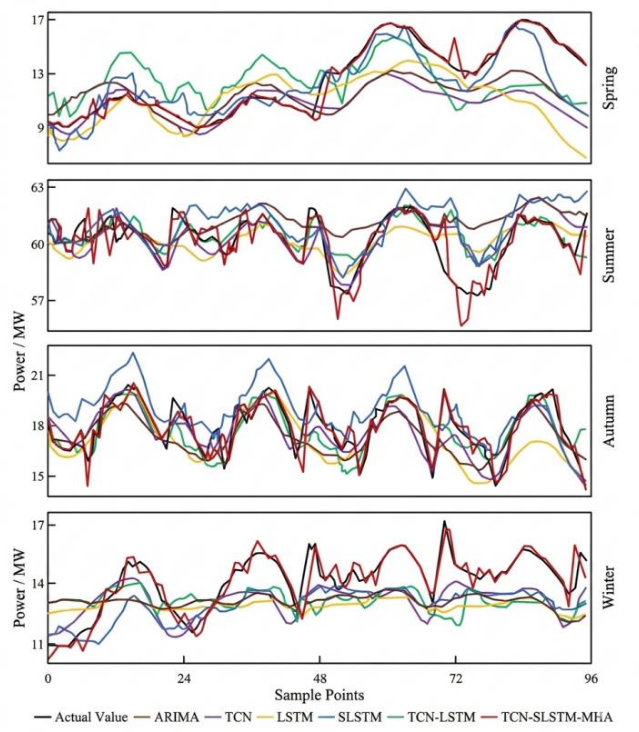


**Figure 8.** Comparison of typical daily load forecasting curves

### 6.1.3. Model Efficiency Analysis

Table 4 compares the training time and parameter size of each model. Due to the introduction of the attention mechanism, the TCN-SLSTM-MHA hybrid model has a slightly larger parameter size than the TCN-LSTM, but its training time remains within an acceptable range (approximately 12.3 minutes per training run), and its prediction speed of 0.02 seconds per sample meets real-time requirements.

Table 4. Comparison of Model Complexity and Efficiency

| Model | Parameter Size (10,000) | Training Time (min/round) | Prediction time (seconds per sample) |
|---|---|---|---|
| ARIMA | - | 0.5 | 0.010 |
| TCN | 86 | 8.7 | 0.015 |
| LSTM | 72 | 9.2 | 0.018 |
| SLSTM | 90 | 10.0 | 0.020 |
| TCN-LSTM | 105 | 11.5 | 0.022 |
| TCN-SLSTM-MHA | 158 | 14.3 | 0.025 |

## 6.2. Multi-objective Optimization Experiment for Energy Storage Capacity

### 6.2.1. Experimental Setup

Based on the prediction results in Section 6.1, the improved NSGA-II algorithm was employed to solve the multi-objective optimization problem, with the objective functions being LCC, PSR, and CEI, and the constraints including power balance and SOC limits (see Section 5 for details). The improved NSGA-II algorithm is as follows: initial population size N = 200; *maximum number of iterations* $G_{max}$ = 300; crossover *probability* $P_c$ is dynamically adjusted according to Equation 29; mutation probability $P_m$ is adjusted according to Equation 30 in the original paper; the selection operator scale is set to 2. The iteration progression is shown in Figure 9. In the early stages of the iteration, the generation distance decreases sharply. By the 50th iteration, the convergence requirement for generation distance has already been met. By the 200th iteration, the generation distance approaches 0, and the obtained solution can be approximated as the Pareto-optimal frontier, indicating that the algorithm possesses good convergence properties. The improved NSGA-II shows significant convergence of the generation distance after approximately 50 iterations and stabilizes by the 200th iteration, indicating that the algorithm can efficiently obtain a high-quality set of non-dominated solutions.

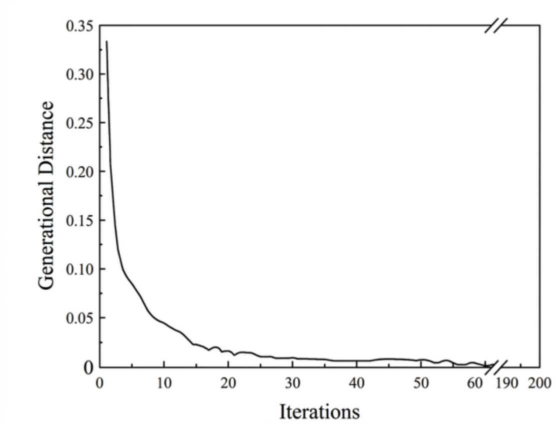


**Figure 9.** Iterative change diagram

Table 5-7 presents the experimental results for LCC, PSR, and CEI obtained using different optimization methods, including single-objective optimization, traditional multi-objective optimization (weighted sum method), and the improved NSGA-II.

As shown in Table 5, the optimization scheme obtained using the improved NSGA-II method achieved a total LCC of 1.4807 million yuan. After balancing economic, reliability, and environmental factors, this value was significantly lower than that of traditional multi-objective optimization methods, with a reduction of up to 15.2%.

Table 5. Comparison and Analysis of LCC for Energy Storage Capacity Optimization Schemes

| **Optimization Method** | **Energy Storage Capacity/kWh** | **Cinv / 10,000 yuan** | **COM / 10,000 yuan** | **Crec / 10,000 yuan** | **LCC/10,000 yuan** |
|---|---|---|---|---|---|
| Single Objective (LCC) | 500 | 130.0 | 25.0 | -6.50 | 148.50 |
| Single Target (PSR) | 700 | 190.0 | 20.0 | -9.50 | 200.50 |
| Single Target (CEI) | 600 | 160.0 | 28.0 | -8.00 | 180.00 |
| Traditional multi-objective optimization | 550 | 152.4 | 29.8 | -7.62 | 174.58 |
| Improved NSGA-II | 510 | 128.6 | 25.9 | -6.43 | 148.07 |

Note: Traditional multi-objective optimization refers to the weighted sum method (in this paper, the LCC weight is set to 0.6, the PSR weight to 0.3, and the CEI weight to 0.1).

As shown in Table 6, the improved NSGA-II method balances economic efficiency while ensuring high reliability. Compared to the traditional multi-objective optimization method, its PSR improves by 4.3%, which validates that the proposed method can better balance economic efficiency and reliability under limited energy storage capacity.

Table 6. Comparison and Analysis of PSR for Energy Storage Capacity Optimization Schemes

| **Optimization Method** | **Energy storage capacity / kWh** | **LOPP/%** | **LOEE/MWh** | **PSR/%** |
|---|---|---|---|---|
| Single objective (LCC) | 500 | 4.5 | 40.0 | 75.0 |
| Single Target (PSR) | 700 | 1.0 | 8.0 | 96.0 |
| Single-target CEI) | 600 | 3.0 | 25.0 | 85.0 |
| Traditional multi-objective optimization | 550 | 3.5 | 30.1 | 83.2 |
| Improved NSGA-II | 510 | 2.8 | 23.6 | 86.8 |

The CEI calculation comprehensively accounts for carbon emissions resulting from grid-purchased electricity and the full lifecycle of energy storage systems. The formula is:

$$CEI = (\lambda_{\mathrm{grid}} \cdot E_{\mathrm{grid}} + \lambda_{\mathrm{bat}} \cdot E_{\mathrm{bat}}) / E_{\mathrm{load}} \tag{40}$$

Where: $\lambda_{\mathrm{grid}}$ is the carbon emission factor per unit of electricity from the grid; $\lambda_{\mathrm{bat}}$ is the carbon emission factor per unit of battery capacity; $E_{\mathrm{grid}}$ is the amount of electricity purchased from the grid; $E_{\mathrm{bat}}$ is the rated battery capacity; $E_{\mathrm{load}}$ is the total load.

Table 7. Comparison and Analysis of CEI for Energy Storage Capacity Optimization Schemes

| **Optimization Method** | **Energy Storage Capacity/kWh** | **Grid Electricity Purchases/MWh** | **CEI /($tCO_2$/MWh)** |
|---|---|---|---|
| Single-objective (LCC) | 500 | 1,100 | 0.600 |
| Single target (PSR) | 700 | 900 | 0.580 |

| | | | |
|---|---|---|---|
| Single Target (CEI) | 600 | 800 | 0.550 |
| Traditional multi-objective optimization | 550 | 1050 | 0.642 |
| Improved NSGA-II | 510 | 980 | 0.562 |

As shown in Table 7, the trend in the CEI is highly correlated with the energy storage capacity configuration. The larger the energy storage capacity, the stronger the system's ability to integrate renewable energy and the lower its reliance on high-carbon power grids; consequently, the CEI value is smaller. The improved NSGA-II method achieved the lowest CEI (0.562 tCO2/MWh) even when the energy storage capacity (510 kWh) was not maximized, indicating that the multi-objective optimization algorithm effectively balanced economic efficiency, reliability, and environmental performance to find a synergistic optimal solution. Compared with traditional multi-objective optimization methods, the proposed improved NSGA-II method reduces the CEI by 12.5%, significantly enhancing the system's environmental performance. This validates the effectiveness of using CEI as an explicit optimization objective.

## 6.3. Validation of Digital Twin Technology

To validate the effectiveness of the digital twin, two sets of comparative experiments were designed:

Scenario 1: Based on raw collected data (uncorrected), TCN-SLSTM-MHA hybrid model predictions, and improved NSGA-II optimization;

Scenario 2: Based on digital twin-corrected data (denoised and time-aligned), TCN-SLSTM-MHA hybrid model predictions, and improved NSGA-II optimization.

This paper selected real-time operational data from the physical system on a representative day—July 15, 2025—and conducted a synchronous comparison with the simulated output of the digital twin model. The accuracy of real-time mapping was quantified by calculating error metrics for key parameters such as energy storage SOC and grid-connection point power. The formulas used included Root Mean Square Error (RMSE) and the correlation coefficient ($R^2$). Experimental results show that the RMSE between the SOC time series output by the digital twin model and the measured values is 1.8 kW, with an $R^2$ of 0.981; the RMSE for grid-connection point power is 4.2 kW, indicating that the model possesses high-fidelity real-time mapping capabilities.

The impact of digital twins on optimization results is shown in Table 8. When optimization was performed using both raw collected data and digital twin-corrected data under the same prediction model, the digital twin correction further reduced investment costs and curtailment rates by 4.2% and O&M costs by 3.4%, respectively, indicating that it can effectively improve data quality and reduce prediction errors. This is because digital twins generate reliable dynamic scenarios through high-fidelity modeling, providing high-quality data for predictions; the TCN-SLSTM-MHA hybrid model achieves high-precision predictions based on twin data, reducing errors in optimization inputs; and the improved NSGA-II multi-objective optimization algorithm utilizes precise prediction results to determine the optimal energy storage capacity, while verifying the feasibility of the solution through digital twins, thereby forming a closed-loop of data-prediction-optimization-verification.

Table 8. Impact of digital twin technology on optimization results

| **Data Source** | **Investment Cost/10,000 RMB** | **Operating and Maintenance Costs (10,000 yuan)** | **Energy Curtailment Rate (%)** |
|---|---|---|---|
| Scenario 1 | 134.2 | 26.8 | 4.8 |
| Option 2 | 128.6 | 25.9 | 4.6 |

## 7. Conclusion

This paper proposes a multi-objective energy storage capacity optimization method that integrates digital twins, the TCN-SLSTM-MHA hybrid model, and an improved NSGA-II algorithm. Specifically, the TCN-SLSTM-MHA hybrid model demonstrates significantly higher accuracy in source-load forecasting compared to the baseline models, with $R^2$ values consistently exceeding 0.92, providing reliable data support for energy storage optimization. By integrating digital twin technology and multi-objective optimization algorithms, the proposed method achieves the coordinated optimization of the energy storage system's LCC, PSR, and CEI. The proposed method exhibits excellent adaptability and robustness under scenarios with high wind and solar penetration rates. The method proposed in this paper achieves high-precision source-load forecasting in wind-solar microgrids, providing accurate data support for energy storage capacity optimization and offering scientific basis and technical support for the rational configuration of energy storage capacity. The limitations of this method include the requirement for high-frequency data synchronization in the digital twin system, which demands high communication real-time performance, and the relatively long training time of the TCN-SLSTM-MHA hybrid model, making it currently unsuitable for ultra-short-term forecasting scenarios. Future work will explore lightweight models and edge computing deployment.

## Acknowledgement
Not applicable.

## References

[1]Bao W, Ge M, Yuan Y, et al. Technical and Economic Optimization of Wind-Solar-Storage Independent Microgrids Considering Demand Response [J]. Acta Energiae Solaris Sinica, 2024, 45(05): 343-350.
[2]Zhao B, Xue P, Deng M, et al.Operation control and simulation study of new energy microgrid system considering windsolar complementarity [J]. China Measurement & Test, 2024, 50(S2): 294-300.
[3]Sun Y, Xing H, Shi Y, et al. Multi-time-scale Adequacy Evaluation and Quantitative Analysis of New Power Systems [J]. Smart Power, 2025, 53(06): 35-42.
[4]Wang Y, Wang H, Hu Y, et al. Optimization of Microgrids and Improvement of Power Quality Based on Wind-Solar Complementary Hybrid Energy Storage Systems [J]. China Electric Power, 2025, 58(07): 162-167.
[5] Cao Y, Zhang H, LI C. Robust Optimization Configuration for Energy Storage System Capacity Considering Uncertainty of Disturbance [J]. Automation of Electric Power Systems, 2024, 48(19): 139-147.
[6]Huang D, Wu B, Shi S, et al. Capacity Optimization of a Hybrid Energy Storage System for Wind Power Fluctuation Suppression Based on CEEMDAN-SAOA [J]. Protection and Control of Power Systems, 2025, 53(15): 59-70.
[7]Mulleriyawage U G K, Shen W X. Optimally sizing of battery energy storage capacity by operational optimization of residential PV-Battery systems: An Australian household case study [J]. Renewable Energy, 2020, 160: 852-864.
[8]Soltani N Y, Nasiri A. Chance-constrained optimization of energy storage capacity for microgrids [J]. IEEE Transactions on Smart Grid, 2020, 11(4): 2760-2770.
[9]Xie P, Cai Z, Liu P, et al. Microgrid system energy storage capacity optimization considering multiple time scale uncertainty coupling [J]. IEEE Transactions on Smart Grid, 2018, 10(5): 5234-5245.
[10] Bailek N, Bouchouicha K, Al-Mostafa Z, et al. A new empirical model for forecasting the diffuse solar radiation over Sahara in the Algerian Big South [J]. Renewable Energy, 2018, 117: 530-537.
[11]Pelikan E, Eben K, Resler J, et al. Wind power forecasting by an empirical model using NWP outputs [C] // 2010 9th International Conference on Environment and Electrical Engineering. IEEE, 2010: 45–48.
[12]Lü X, Lu T, Kibert C J, et al. Modeling and forecasting energy consumption for heterogeneous buildings using a physical–statistical approach [J]. Applied Energy, 2015, 144: 261–275.
[13]Gupta P, Singh R. PV power forecasting based on data-driven models: a review [J]. International Journal of Sustainable Engineering, 2021, 14(6): 1733–1755.
[14]Kisvari A, Lin Z, Liu X. Wind power forecasting–A data-driven method along with gated recurrent neural network [J]. Renewable Energy, 2021, 163: 1895–1909.
[15]Zhu J, Dong H, Zheng W, et al. Review and Prospect of Data-Driven Techniques for Load Forecasting in Integrated Energy Systems [J]. Applied Energy, 2022, 321: 119269.
[16]Lin S, Feng X, Liang W, et al. Research Status and Prospects of Uncertain Optimal Dispatch Methods for Renewable Energy Power Systems [J]. Automation of Electric Power Systems, 2024, 48(10): 20-41.
[17]Bai S, Kolter J Z, Koltun V. An empirical evaluation of generic convolutional and recurrent networks for sequence modeling [J]. arXiv preprint arXiv:1803.01271, 2018.
[18]Hochreiter S, Schmidhuber J. Long Short-Term Memory [J]. Neural Computation, 1997, 9(8): 1735-1780.
[19] Limouni T, Yaagoubi R, Bouziane K, et al. Intelligent real-time control strategy and power management based on MPC and LSTM-TCN model for standalone DC microgrid with energy storage [J]. International Journal of Electrical Power & Energy Systems, 2025, 169: 110761.
[20]Zhang Y, Zhang Y, Yang Z, et al. GVMD-TSNE-TCN-LSTMre Short Term Forecast Method for Photovoltaic Power Generation Based on Incremental Learning and Gorilla Optimization [J]. Acta Energiae Solaris Sinica, 2025, 46(07): 690-700.
[21]Do Amaral J V S, Dos Santos C H, Montevechi J A B, et al. Energy digital twin applications: a review [J]. Renewable and Sustainable Energy Reviews, 2023, 188: 113891.
[22]Semeraro C, Olabi A G, Aljaghoub H, et al. Digital twin application in energy storage: Trends and challenges [J]. Journal of Energy Storage, 2023, 58: 106347.
[23] Zhang D, Liu H, Li C. Digital Twin-based Multi-objective Optimal Scheduling for Hybrid Microgrids [J]. Acta Energiae Solaris Sinica, 2025, 46(02): 184-192.
[24]Ding L, Chen Y, Xiao T, et al. Topology-Aware Fault Diagnosis for Microgrid Clusters with Diverse Scenarios Generated by Digital Twins [J]. Applied Energy, 2025, 378: 124794.
[25]Ali S M, Khan B, Ullah Z. Deep Learning-Enabled Digital Twins for Prosumers: A Holistic Energy Management Framework for Smart Grids Using Deep Reinforcement Learning and Big Data Analytics [J]. International Journal of Energy Research, 2025, 2025(1): 6618907.
[26]You M, Wang Q, Sun H, et al. Digital twins-based day-ahead integrated energy system scheduling under load

and renewable energy uncertainties [J]. Applied Energy, 2022, 305: 117899.
[27]Chen Y, Meng H, Zhang H, et al. A Digital Twin Model for Electricity/Heat/Gas Multi-energy Systems and Its Optimal Operation Strategy [J]. Renewable Energy Resources , 2025, 43(06): 820-828.